Journal of Research in Science and Engineering (JRSE)
ISSN: 1656-1996 Volume-6, Issue-11, November 2024
DOI: 10.53469/jrse.2024.06(11).03

Analysis and Modeling of Four-Quadrant PWM Rectifier

Yingqi Yu, Chunyan Wang

Jiangsu Maritime Insinuate, School of Information Technology, Nanjing, Jiangsu, China

Abstract: ***Different from the traditional AC/DC converters, the four-quadrant converters are widely used in modern AC power transmission systems because of their advantages such as two-way flow of energy, adjustable power factor on the grid side, and stable voltage on the DC side [1]. In this paper, the mathematical model of four-quadrant PWM rectifier is presented, and on this basis, the constant-frequency double closed-loop control strategy is adopted to control the DC voltage and the power factor of the grid side. The determination method of voltage and current PI regulator parameters is analyzed, and the influence of ac side inductance and DC side capacitance on the whole system is pointed out, and the design method is given. Through the establishment of simulation model under MATLAB/ Simulink, it is proved that this model can realize the DC voltage and power factor control at the side of the network, has a good load regulation ability, and can switch between the rectifier mode and the inverter mode, realizing the two-way flow of energy. This paper has some guiding effect on the design of four-quadrant PWM rectifier.***

Keywords: Four-quadrant PWM rectifier, Double closed loop control, Bidirectional transfer of energy.

1. Introduction

In modern AC drive systems, the AC-DC-AC voltage-source inverter main circuit topology is widely adopted. Due to the use of diode-based uncontrolled rectification in traditional circuit structures, energy cannot flow bidirectionally, resulting in most of the generated pump-up voltage being dissipated in braking resistors, leading to significant energy wastage. The Four-Quadrant PWM Rectifier (VSR) is extensively studied and applied in engineering owing to its advantages such as stable DC-side voltage, near-sinusoidal grid-side current, adjustable power factor, and bidirectional energy flow. The control strategies for PWM rectification are primarily categorized into "indirect current control" and "direct current control". "Direct current control" has rapidly developed due to its fast current response and strong robustness. Commonly used methods include hysteresis-band PWM current control and fixed switching frequency PWM current control. Among these, fixed switching frequency PWM current control is widely applied due to its simple algorithm, clear physical meaning, and ease of implementation. A voltage-current double closed-loop cascade control is employed, with feedforward decoupling used to decouple the currents in the dq coordinate system. Simulation verification is conducted in Matlab/Simulink.

2. The Basic Principle of Four-Quadrant PWM Rectifier

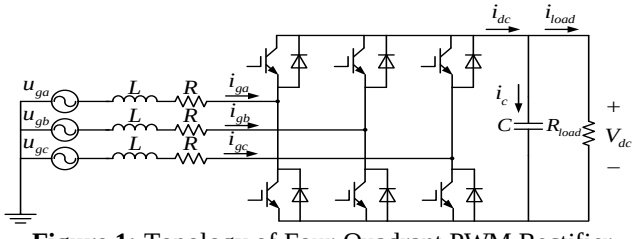

Figure 1: Topology of Four-Quadrant PWM Rectifier

The mathematical model of the grid-side PWM converter is the foundation for analyzing and controlling its dynamic and steady-state operations. The main circuit of the grid-side PWM converter is shown in Figure 1 [2].

In Figure 1, u_{ga}, u_{gb}, u_{gc} are the phase voltages of the three-phase grid;i_{ga}, i_{gb}, i_{gc} are the three-phase input currents of the grid-side PWM converter; V_{dc} is the DC bus voltage; $i_{load}$is the load current on the DC side; i_{dc} is the output current from the DC side;L is the inductance of each phase's incoming reactor;Ris the resistance of each phase's line, including the reactor's resistance; C is the DC bus capacitance.

Assuming that the power devices in Figure 1 are ideal switches, then based on the topology of the grid-side PWM converter shown in Figure 1 and applying Kirchhoff's voltage and current laws, we can derive:

$$\begin{aligned} &u_{ga} - i_{ga}R - L\frac{di_{ga}}{dt} - S_aV_{dc} \\ &= u_{gb} - i_{gb}R - L\frac{di_{gb}}{dt} - S_bV_{dc} \\ &= u_{gc} - i_{gc}R - L\frac{di_{gc}}{dt} - S_cV_{dc} \\ &C\frac{dV_{dc}}{dt} = S_ai_{ga} + S_bi_{gb} + S_ci_{gc} - i_{load} \end{aligned} \tag{1}$$

In the equation: S_a, S_b, S_c are the switching functions of the three-phase bridge arms.S_k =1 indicates that the upper switch of the corresponding bridge arm is on and the lower switch is off; S_k =0indicates that the lower switch of the corresponding bridge arm is on and the upper switch is off, (k = a, b, c).

In a three-phase system without a neutral line, the sum of the three-phase currents is zero, i.e.,:

$$i_{ga} + i_{gb} + i_{gc} = 0 \tag{2}$$

Substitute the above equation into Equation 1.

$$\begin{aligned}
\frac{di_{ga}}{dt} &= -\frac{R}{L}i_{ga} + \frac{1}{L}\left[\left(u_{ga} - \frac{(u_{ga}+u_{gb}+u_{gc})}{3}\right) - \left(S_a - \frac{(S_a+S_b+S_c)}{3}\right)V_{dc}\right] \\
\frac{di_{gb}}{dt} &= -\frac{R}{L}i_{gb} + \frac{1}{L}\left[\left(u_{gb} - \frac{(u_{ga}+u_{gb}+u_{gc})}{3}\right) - \left(S_b - \frac{(S_a+S_b+S_c)}{3}\right)V_{dc}\right] \\
\frac{di_{gc}}{dt} &= -\frac{R}{L}i_{gc} + \frac{1}{L}\left[\left(u_{gc} - \frac{(u_{ga}+u_{gb}+u_{gc})}{3}\right) - \left(S_c - \frac{(S_a+S_b+S_c)}{3}\right)V_{dc}\right] \\
C\frac{dV_{dc}}{dt} &= S_a i_{ga} + S_b i_{gb} + S_c i_{gc} - i_{lood}
\end{aligned} \tag{3}$$

In most cases, the three-phase grid voltages are basically balanced. Therefore, when studying the operation of the grid-side PWM converter under normal grid conditions, it is assumed that the three-phase grid voltages are balanced, that is:

$$\mathrm{u_{ga}} + \mathrm{u_{gb}} + \mathrm{u_{gc}} = 0 \tag{4}$$

Substituting into Equation 3, we can obtain:

$$\begin{cases}
\frac{di_{ga}}{dt} = -\frac{R}{L}i_{ga} + \frac{1}{L}\left[u_{ga} - \left(S_a - \frac{(S_a+S_b+S_c)}{3}\right)V_{dc}\right] \\
\frac{di_{gb}}{dt} = -\frac{R}{L}i_{gb} + \frac{1}{L}\left[u_{gb} - \left(S_b - \frac{(S_o+S_b+S_c)}{3}\right)V_{dc}\right] \\
\frac{di_{gc}}{dt} = -\frac{R}{L}i_{gc} + \frac{1}{L}\left[u_{gc} - \left(S_c - \frac{(S_a+S_b+S_c)}{3}\right)V_{dc}\right] \\
C\frac{dV_{dc}}{dt} = S_a i_{ga} + S_b i_{gb} + S_c i_{8c} - i_{load}
\end{cases} \tag{5}$$

To simplify the above equation, let

$$\begin{cases}
V_a = \left(S_a - \frac{S_a+S_b+S_c}{3}\right)V_{dc} \\
V_b = \left(S_b - \frac{S_a+S_b+S_c}{3}\right)V_{dc} \\
V_c = \left(S_c - \frac{S_a+S_b+S_c}{3}\right)V_{dc}
\end{cases} \tag{6}$$

The simplified equation is

$$\begin{cases}
\frac{di_a}{dt} = -\frac{R}{L}i_a + \frac{1}{L}[u_a - V_a] \\
\frac{di_b}{dt} = -\frac{R}{L}i_b + \frac{1}{L}[u_b - V_b] \\
\frac{di_c}{dt} = -\frac{R}{L}i_c + \frac{1}{L}[u_c - V_c]
\end{cases} \tag{7}$$

Next, we will perform a coordinate transformation on the above equation, converting it from the original stationary abc coordinate system to the rotating dq0 coordinate system.

$$u_{dq} = T_{abc-dq} \cdot u_{abc} = L \cdot T_{abc-dq} \cdot \frac{di_{abc}}{dt} + R \cdot T_{abc-dq} \cdot i_{abc} + T_{abc-dq} \cdot V_{abc} \tag{8}$$

In the equation: $\mathrm{T_{abc-dq}}$represents the transformation matrix that converts from the stationary abc coordinate system to the rotating dq0 coordinate system, namely

$$T_{abc-dq} = \sqrt{\frac{2}{3}}\begin{bmatrix} cos\,\omega t & cos\left(\omega t - \frac{2}{3}\pi\right) & cos\left(\omega t + \frac{2}{3}\pi\right) \\ -sin\,\omega t & -sin\left(\omega t - \frac{2}{3}\pi\right) & -sin\left(\omega t + \frac{2}{3}\pi\right) \end{bmatrix} \tag{9}$$

Thus, we can obtain,

$$u_{dq} = L \cdot \frac{d(T_{abc-dq} \cdot i_{abc})}{dt} - L \cdot T'_{abc-dq} \cdot i_{abc} + R \cdot T_{abc-dq} \cdot i_{abc} + T_{abc-dq} \cdot V_{abc} \tag{10}$$

i.e.,

$$\begin{bmatrix} u_d \\ u_q \end{bmatrix} = \begin{bmatrix} L \cdot \frac{di_d}{dt} - \omega \cdot L \cdot i_q + R \cdot i_d + V_d \\ L \cdot \frac{di_q}{dt} + \omega \cdot L \cdot i_d + R \cdot i_q + V_q \end{bmatrix} \tag{11}$$

Thus, the output voltage of the PWM rectifier can be obtained.

$$V_{dq} = \begin{bmatrix} V_d \\ V_q \end{bmatrix} = \begin{bmatrix} -L \cdot \frac{di_d}{dt} + \omega \cdot L \cdot i_q - R \cdot i_d + u_d \\ -L \cdot \frac{di_q}{dt} - \omega \cdot L \cdot i_d - R \cdot i_q + u_q \end{bmatrix} \tag{12}$$

Where $u_{dq} = \begin{bmatrix} \sqrt{\frac{3}{2}} \cdot U_{max}[] \\ 0 \end{bmatrix}$ represents the maximum value of the phase voltage.

Next, a simulation model will be built based on the derived mathematical expressions.

2.1 Main Topology Model of the Converter

The main topology model of the converter is constructed using discrete components, as shown in Figure 2.

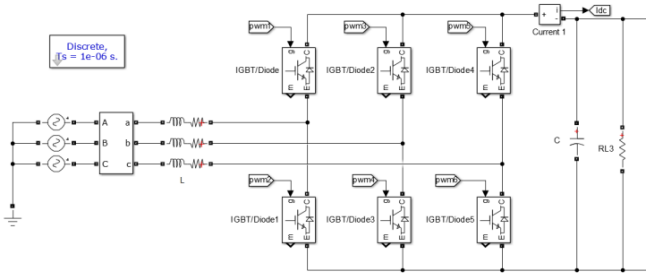

Figure 2: Simulation Model of the Converter's Main Topology

The three-phase voltage source consists of three 220V RMS, 50Hz AC voltage sources with a phase difference of 120° between each other. The three-phase rectifier section employs six ideal IGBT switches, each with an anti-parallel diode.

2.2 Control Loop

Based on the previous derivations, the control block diagram of the system can be obtained. The control block diagram in MATLAB/Simulink is shown in Figure 3.

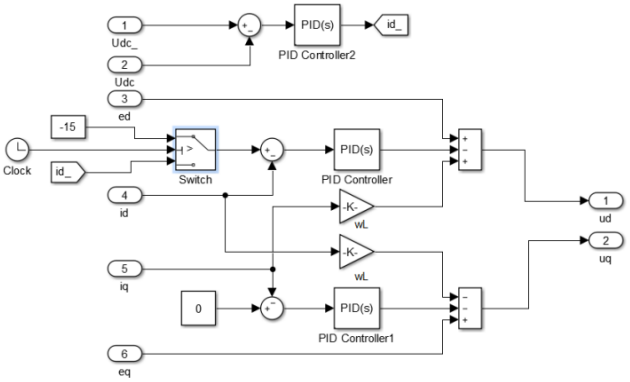

Figure 3: Simulation Model of the Control Block Diagram

A dual closed-loop control strategy of voltage and current is adopted, where the voltage loop serves as the outer loop and the current loop as the inner loop. The output of the voltage loop is used as the reference for the current loop.

2.3 Phase-Locked Loop (PLL)

The phase-locked loop (PLL) employs a software-based phase-locking method using a self-constructed module. It takes three-phase voltage as input and outputs the phase angle and frequency. The schematic diagram of the PLL is shown in Figure 4, which utilizes PI (Proportional-Integral) control to form a feedback loop. The internal structure of the PLL in MATLAB/Simulink is depicted in Figure 5.

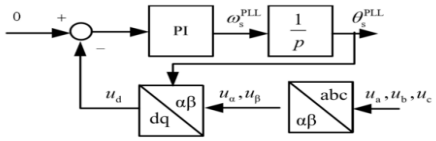

Figure 4: A Software-Controlled Phase-Locked Loop (PLL)

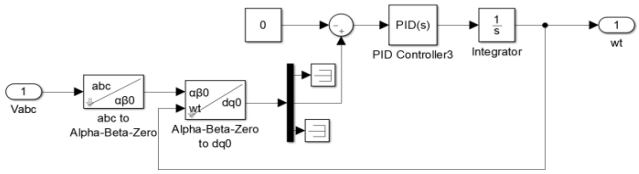

Figure 5: Simulation Model of the Constructed Phase-Locked Loop (PLL)

2.4 PWM Generator

The PWM generator employs a self-constructed SPWM (Sine Pulse Width Modulation) generating circuit. The SPWM generating circuit in MATLAB/Simulink is shown in Figure 6.

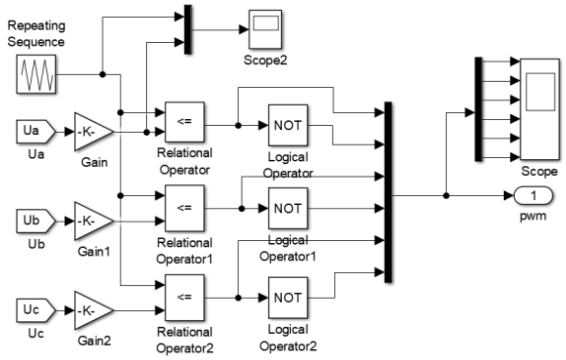

Figure 6: Simulation Model of SPWM Generator

Using a triangular wave with a frequency of 100 kHz as the carrier signal, the standardized abc three-phase voltages are compared with the triangular carrier. When the input phase voltage is less than the value of the triangular carrier, the PWM generator outputs a high level, controlling the switch to turn on. When the input phase voltage is greater than the value of the triangular carrier, the PWM generator outputs a low level, controlling the switch to turn off.

2.5 Protection Circuit

The protection circuit includes overvoltage protection for the output voltage and overcurrent protection for the input current, and its block diagram is shown in Figure 7.

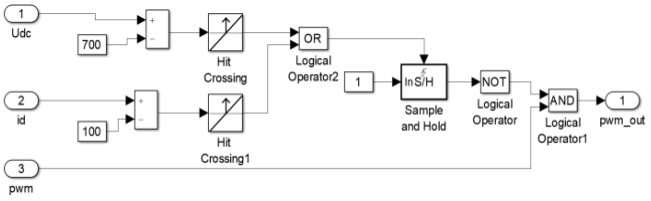

Figure 7: Simulation Model of the Protection Circuit

The output voltage protection value is set at 700V. When the output voltage exceeds 700V, the Hitcrossing module detects a zero-crossing signal, triggering a pulse. The sample-and-hold circuit can convert this pulse signal into a level signal. In the event of an overvoltage, the fault protection circuit outputs a high level. After inversion, this signal is ANDed with the PWM signal to block it. With the PWM signal blocked, the three-phase PWM rectifier degrades into a three-phase uncontrolled rectifier circuit. This protection method is simple in logic and quick in action. In practical circuits, FPGAs are commonly used for PWM hardware protection.

The principle of input current overcurrent protection is the same as that of output voltage overvoltage protection.

3. Circuit Parameter Design

3.1 AC-side Inductance Parameter Design

Since the value of the AC-side inductance not only affects the dynamic and static responses of the current loop but also constrains the output power, power factor, and DC-side voltage of the Voltage Source Rectifier (VSR), the selection of the AC-side inductance is crucial. The selection should adhere to the following principles [3]: while maximizing the suppression of grid-side current harmonics, it must also meet the tracking requirements of the maximum current.

Ignoring the influence of the AC-side resistance, we can obtain the voltage equation for phase a:

$$L\frac{di_a}{dt} = e_a - u_{dc}[s_a - \frac{1}{3}(s_a + s_b + s_c)] \quad (13)$$

This can be represented using an incremental equation as follows:

$$\Delta i_a = \frac{T_s}{L}\{e_a - u_{dc}[s_a - \frac{1}{3}(s_a + s_b + s_c)]\} \quad (14)$$

In the equation, T_s represents the PWM switching period, u_{dc} represents the DC bus voltage, and s_a, s_b and s_c represent the switching state functions of the a, b, and c phases, respectively.

The pulsation value of the current should be less than the allowed maximum current pulsation value, so the AC-side inductance must be sufficiently large to suppress current pulsation. Near the peak value, current pulsation is most severe, therefore it should be satisfied that:

$$\Delta i_a = \frac{T_s}{L}(\sqrt{2}e_a + \frac{2}{3}u_{dc}) \le \Delta i_{a\_max} \quad (15)$$

Namely,

$$L \ge \frac{T_s}{\Delta i_{a\_max}}(\sqrt{2}e_a + \frac{2}{3}u_{dc}) \quad (16)$$

In the equation, e_a represents the root mean square (RMS) value of the grid-side current, and Δi_{a_max} represents the allowed maximum current pulsation value.

3.2 DC-side Capacitor Parameter Design

The capacitor on the DC side plays a direct role in the stability of the DC voltage. The larger the capacitance value, the smaller the ripple on the DC side, but at the same time, the larger the volume of the capacitor. Therefore, the selection of the DC-side capacitor is a compromise between volume and ripple size. The smallest capacitance value should be selected as much as possible while meeting the ripple requirements. the minimum capacitance value that meets the ripple requirement is:

$$C \geqslant \frac{3\times L\times r_i\times I_{sm}^2}{r_v U_{dc}^2} \tag{17}$$

In the equation: r_i is the ripple coefficient of the DC current; r_v is the ripple coefficient of the DC voltage; I_{sm} is the amplitude of the phase current.

4. PI Controller Parameter Design

In this paper, a dual closed-loop control strategy is adopted to regulate the DC-side voltage and AC-side current, where the current loop serves as the inner loop and the voltage loop as the outer loop. The output of the voltage loop is used as the reference value for the current loop.

4.1 PI Parameter Design for the Current Inner Loop

The control block diagram of the current loop is shown in Figure 8. This figure represents the control block diagram of the current loop under ideal conditions (without considering delays). In practical applications, there will be certain delays in the sampling circuit and PWM generation circuit. Therefore, it is necessary to incorporate the necessary delay elements into the process of designing the PI parameters for both the current loop and the voltage loop. By equating all delays, including sampling delay and PWM delay, to 1.5 PWM cycles and representing them as an inertial element, we obtain the control block diagram of the current loop considering the delay elements, as shown in Figure 9.

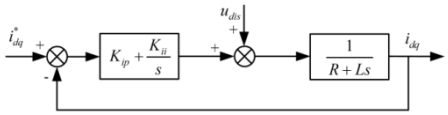

Figure 8: Control Block Diagram of the Current Loop under Ideal Conditions

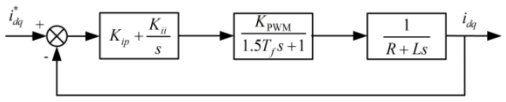

Figure 9: Control Block Diagram of the Current Loop Considering Delay Elements

In Figure 9, T_s represents the sampling period of the current inner loop (i.e., the PWM switching period), and K_{PWM} represents the equivalent gain of the PWM. Due to the requirement for fast current tracking performance in the current inner loop, a typical system design approach is chosen for the current regulator. From Figure 9, the transfer function of the current inner loop is derived as [4]:

$$W_{oi}(s)=\frac{K_{\mathrm{PWM}}K_{ip}\left(s+\frac{K_{ii}}{K_{ip}}\right)}{sL(1.5T_s s+1)\left(s+\frac{R}{L}\right)} \tag{18}$$

To simplify the transfer function of the current loop based on the principle of zero-pole cancellation, it only needs to satisfy:

$$\frac{K_{ii}}{K_{ip}}=\frac{R}{L} \tag{19}$$

The simplified transfer function of the current loop is:

$$W_{oi}(s)=\frac{K_{\mathrm{PWM}}K_{ip}}{sL(1.5T_s s+1)} \tag{20}$$

In the closed-loop transfer function, by taking the damping ratio as 0.707, we can obtain:

$$\begin{cases} K_{iP}=\dfrac{L}{3T_s K_{\mathrm{PWM}}} \\ K_{il}=\dfrac{R}{3T_s K_{\mathrm{PWM}}} \end{cases} \tag{21}$$

4.2 PI Parameter Design for the Voltage Outer Loop

The output of the voltage loop serves as the setpoint for the current loop, as shown in Figure 10. Generally, the voltage loop is designed with a greater emphasis on anti-interference. Therefore, in engineering practice, the voltage loop is typically tuned to behave like a typical system.

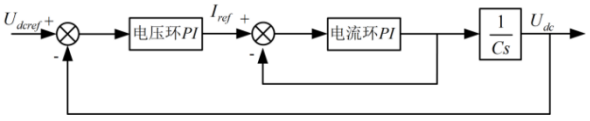

Figure 10: Control Block Diagram of the Voltage Loop

5. Analysis of Simulation Results

5.1 Dynamic and Steady-State Simulation Analysis

The overall block diagram of the simulation is shown in Figure 11.

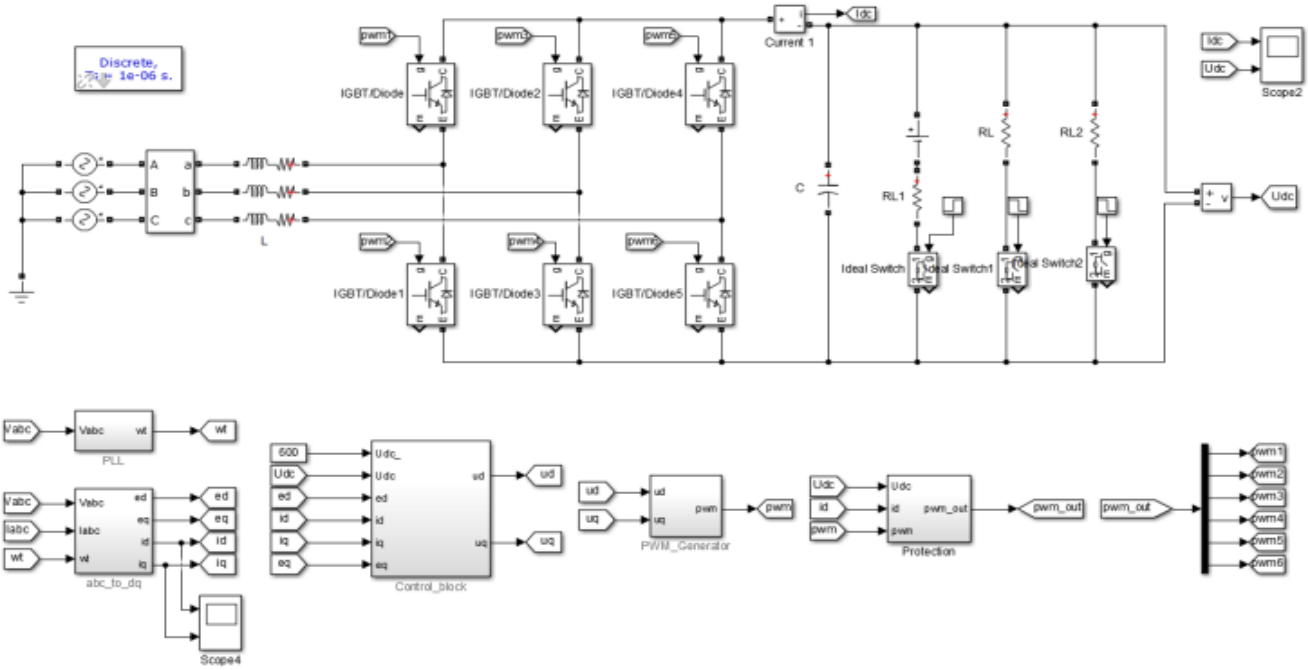

Figure 11: Overall Block Diagram of the Simulation

The parameters for the circuit simulation are shown in Table 1.

Table 1: Circuit Parameters in the Simulation

Parameters	AC Phase Voltage (RMS)
AC Phase Voltage (RMS)	220V
DC Voltage	600V
Switching Frequency	100kHz
Input Side Power Factor	1

Set the DC output voltage to 600V and the power factor on the AC side to 1. Figure 12 shows the dynamic time-domain waveform of the DC voltage.

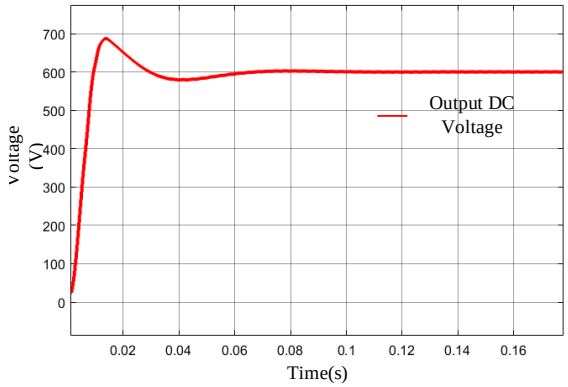

Figure 12: Dynamic Waveform of DC Voltage

From Figure 12, it can be observed that the dynamic adjustment time of the output voltage on the DC side is approximately 0.08s, with a voltage overshoot of about 80V during the rising process. By zooming in on the steady-state process, we obtain Figure 13. It can be seen that in the steady state, the output voltage stabilizes at 600V, with a voltage ripple of around 0.5V.

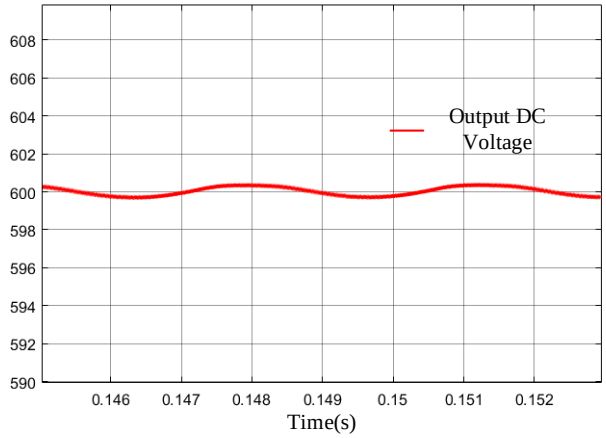

Figure 13: Steady-state Waveform of DC Voltage

Observing the voltage and current on the AC side, we obtain Figure 14. It can be seen that the power factor on the AC side is 1, and the steady state is reached within 0.02s.

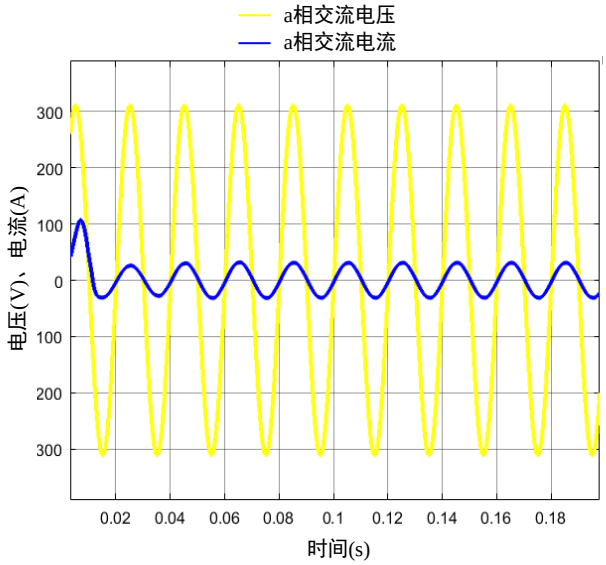

Figure 14: Waveforms of AC Voltage and Current in Steady

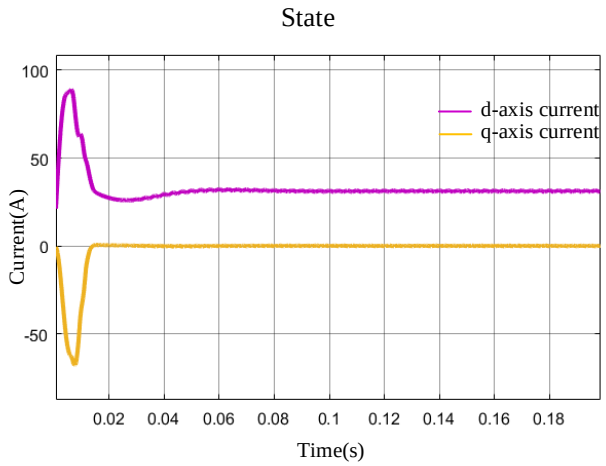

Figure 15: d-axis Current and q-axis Current in Steady State

Figure 15 shows the d-axis current and q-axis current after dq transformation. It can be seen that both currents reach steady state within 0.06s, and the q-axis current is 0 in the steady state (indicating a power factor of 1 on the AC side).

5.2 Simulation Analysis of Load Regulation Capability

To verify the regulation characteristics of the simulation model, a sudden load change was introduced into the circuit. The load resistance was added at the moment of 0.2s (transitioning from heavy load to light load).

Figure 16 shows the change in output voltage when the load is suddenly reduced. From Figure 16, it can be seen that when the load is suddenly reduced, the output voltage experiences a brief increase before stabilizing back to the original 600V under the control of the controller. Figure 17 displays the waveforms of AC side voltage and current, indicating that both AC current and voltage reach steady state after about 0.06s (three cycles) of adjustment. Figure 18 presents the waveforms of d-axis current and q-axis current. During the load transient, it can be observed that the q-axis current remains at 0 while only the d-axis current changes.

This confirms that the model has strong voltage regulation capability when the load undergoes sudden changes.

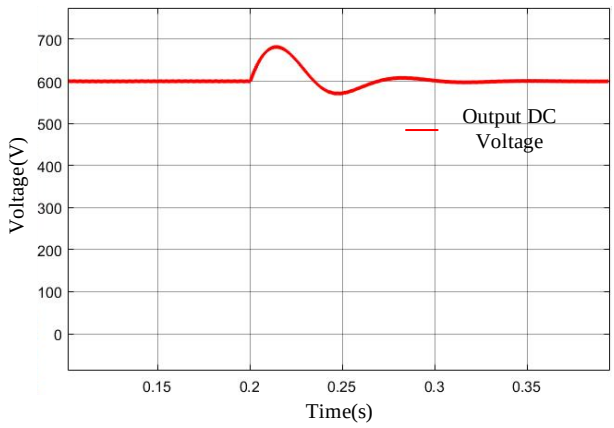

Figure 16: DC Voltage Waveform During Load Switching

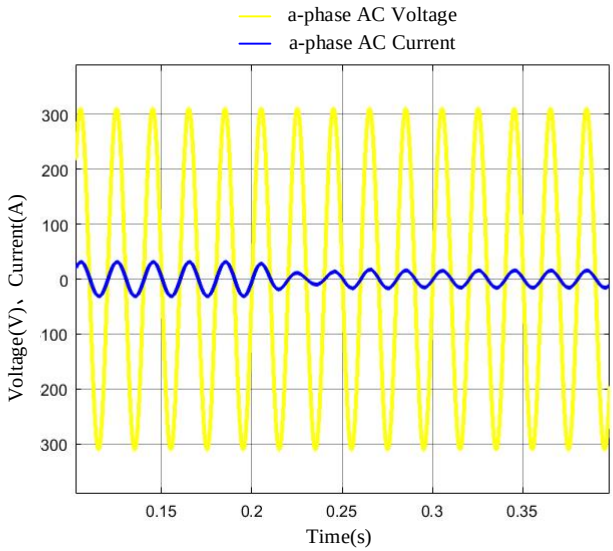

Figure 17: AC Voltage and AC Current Waveforms During Load Switching

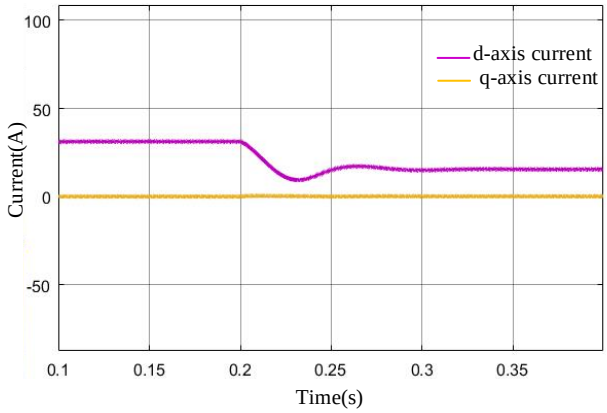

Figure 18: d-axis Current and q-axis Current During Load Switching

6. Conclusion

This paper presents a mathematical model of a four-quadrant PWM rectifier and employs a constant frequency double closed-loop control strategy to regulate the DC voltage and grid-side power factor based on this model. It analyzes the method for determining the parameters of the voltage and current PI controllers, highlights the influence of the selection of AC-side inductance and DC-side capacitance on the overall system, and provides a design approach. Through the establishment of a simulation model in MATLAB/Simulink, it is confirmed that this model can effectively control the DC voltage and grid-side power factor, possesses good load regulation capabilities, and can switch between rectification mode and inversion mode, enabling bidirectional energy flow.

References

[1] Li Guiliang, Luo Xinyuan, Tang Biao, et al. Research on High Power Quality Control of Single-Phase PWM Rectifier [J]. Power Electronics Technology, 2023, 57(06): 1-5.

[2] Gu Changbin, Wang Chenchen, Wang Kun, et al. Virtual Vector Control Strategy for Single-Phase PWM Rectifier [J]. Electrical Engineering, 2019, 34(S1): 202-211. DOI: 10.19595/j.cnki.1000-6753.tces.180516.

[3] Tao M, Lei H, Zhipeng M, et al. Analysis and Calculation of Inductor Parameter for PWM rectifier [C]//Journal of Physics: Conference Series. IOP Publishing, 2023, 2589(1): 012036.
[4] Varaprasad G V M, Nuvvula S S R, Kumar P P, et al. Author Correction: Design and implementation of single DC-link based three-phase multilevel inverter with CB-PWM techniques[J].Scientific Reports, 2024, 14(1):21901-21901.